Removing Aggregates from Single-Walled Carbon Nanotube Samples by Magnetic Purification

ARTICLE *in* THE JOURNAL OF PHYSICAL CHEMISTRY C · FEBRUARY 2014

Impact Factor: 4.77 · DOI: 10.1021/jp411941k

THE JOURNAL OF PHYSICAL CHEMISTRY C

Article

pubs.acs.org/JPCC

Removing Aggregates from Single-Walled Carbon Nanotube Samples by Magnetic Purification

Saunab Ghosh, Sergei M. Bachilo, and R. Bruce Weisman*

Department of Chemistry and R.E. Smalley Institute for Nanoscale Science and Technology, Rice University, 6100 Main Street, Houston, Texas 77005, United States

Supporting Information

ABSTRACT: Purification of raw single-walled carbon nanotube (SWCNT) material remains an important challenge in nanotube research and applications. We describe here a simple but effective purification method that uses permanent magnets to remove many nanotube aggregates, as well as residual metallic catalyst, from aqueous suspensions of surfactant-coated SWCNTs. Samples have been characterized by optical absorption, fluorescence, and Raman spectroscopies; atomic force microscopy and near-infrared fluorescence microscopy; and thermogravimetric analysis. It is found that magnetic purification reduces absorption backgrounds and increases average fluorescence efficiencies to levels comparable to those in ultracentrifuged samples. The ratio of individualized SWCNTs to aggregates in magnetically processed HiPco samples is estimated to be approximately 4:1. As compared to ultracentrifugation, magnetic processing promises major advantages in cost, simplicity, energy consumption, and scalability.

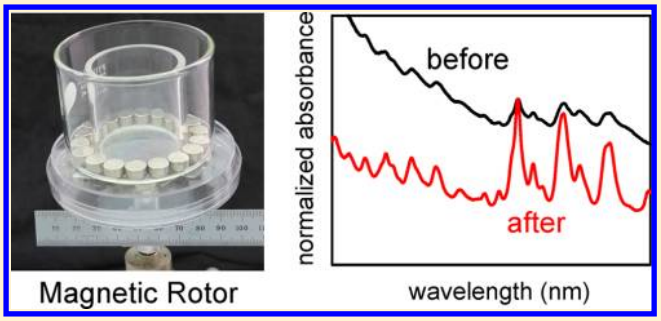

1. INTRODUCTION

The remarkable physical and chemical properties of single-walled carbon nanotubes (SWCNTs) have motivated intense research efforts in science and engineering. A key step in most SWCNT studies or application development is the processing of raw reactor product to obtain individualized nanotubes free of the nanotube aggregates, carbonaceous impurities, and residual metallic growth catalyst that can constitute substantial portions of the as-grown material.[1] It is particularly challenging to process and purify samples without causing physical or chemical damage to the nanotubes themselves. Such damage is most evident in changes to their optical properties, such as increased Raman D/G band ratios,[2] broadened or lowered contrast absorption peaks,[3] or reduced near-infrared (IR) fluorescence efficiency.[4] The first step in purification is disentangling and debundling the components of a solid raw SWCNT sample, typically by ultrasonic dispersion in an aqueous surfactant solution.[5] Nanotube damage in this step can be limited by minimizing the duration and intensity of sonication. The resulting dispersions are then commonly ultracentrifuged to separate denser aggregates and impurities from the individually suspended SWCNTs, which are recovered in the supernatant.[6]

We describe here a simple, inexpensive, and scalable alternative to the centrifugation step that uses permanent magnets to remove many impurities and aggregates from nanotube suspensions. Although there are several prior reports of magnetic purification of nanotube samples,[7−10] those studies were focused only on the removal of metallic impurities. By using a range of optical and AFM measurements, we demonstrate that our magnetic processing method also removes nanotube aggregates as effectively as ultracentrifugation, giving purified suspensions with sharp absorption spectra and high fluorescence efficiencies. Such samples are suitable for subsequent advanced processing by methods such as ion exchange chromatography, density gradient ultracentrifugation, or gel-based structural sorting.[11−18]

2. EXPERIMENTAL SECTION

2.1. Approach. Our method arose from initial observations that a strong permanent magnet placed at the bottom of a vial of suspended raw HiPco SWCNTs slowly attracts some components from the sample. The resulting supernatant layer has less background absorption than the original suspension but shows pronounced resonant absorption peaks and strong near-IR fluorescence. To achieve more efficient magnetic purification, we have constructed special processing containers (shown in Figure 1) in which the liquid sample flows slowly over multiple magnets. This scheme allows all portions of the sample to encounter high field regions near the magnet surfaces. A raw SWCNT sample is first dispersed in surfactant solution using moderate tip sonication. Magnetic purification then proceeds in two stages. In the first, the dispersion is treated for 30 min in a low-speed rotor chamber containing disk magnets (Figure 1a). This removes strongly ferromagnetic particles, apparently including many nanotube aggregates, by depositing them

Received: December 5, 2013
Revised: January 28, 2014
Published: January 29, 2014

   dx.doi.org/10.1021/jp411941k | J. Phys. Chem. C 2014, 118, 4489−4494

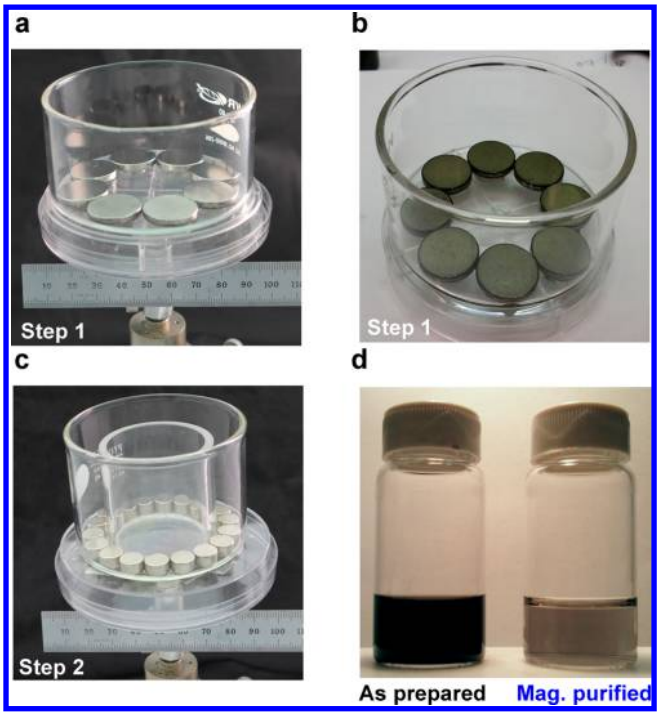

Figure 1. (a) Photograph of the first-stage magnetic purification device. The cell with eight permanent magnets is rotated slowly by the dc gear motor seen at the bottom of the frame. (b) First-stage purification cell after sample treatment. The dark areas are deposits of ferromagnetic materials removed by the treatment. (c) Photograph of the second-stage magnetic purification device. (d) Photographs of vials containing SWCNT suspensions before (left) and after (right) magnetic purification.

onto the magnet edges. Figure 1b shows the dark deposits generated in this stage. Nearly all of the supernatant is then withdrawn from the container and further purified in a second stage that uses an array of smaller diameter disk magnets and a slowly rotating annular sample chamber designed to keep the liquid suspension close to the magnet edges (Figure 1c). After a treatment of approximately 4.5 h, ~90% of the liquid volume from the second processing step is decanted to obtain the purified SWCNT suspension shown in Figure 1d.

2.2. SWCNT Sample Dispersion. HiPco SWCNTs used in this study were taken from two batches (HPR 188.4 and 195.1) produced in the Rice University reactor.[19] SWCNTs produced by the CoMoCAT process were obtained from SouthWest NanoTechnologies, Inc. (type SG65), and raw SWCNTs produced by the plasma torch process were obtained from Raymor Nanotech. Approximately 1.5 mg of unprocessed nanotubes were added to a glass vial containing 10 mL of aqueous 1% (w/v) sodium deoxycholate (DOC) or sodium dodecylbenzenesulfonate (SDBS) (99% purity from Fisher Scientific). The sample was ultrasonically dispersed using a Microson XL ultrasonic cell disrupter equipped with a 3 mm probe tip and set for 6 W output power. We sonicated for 20 min using a duty cycle of 30 s on, 30 s off while the vial was immersed in a room-temperature water bath to prevent overheating. Identically prepared samples used for comparison with magnetic purification were further treated by centrifugation for 5 h at 40 000 rpm (171 000*g* max) in a model MLS-50 rotor and Optima Max ultracentrifuge (Beckman).

2.3. Magnetic Purification Processing. We constructed two simple devices for sequential magnetic purification of the SWCNT dispersions (see Figure 1). The first-stage device consisted of a glass crystallizing dish (80 mm diameter, 40 mm deep), at the bottom of which we placed a circular array of eight nickel-plated neodymium disk magnets (each 20 mm diameter, 3 mm thick, N48 strength). These were held in position by magnetic attraction to a set of eight thin steel retaining plates located under the dish's bottom surface. The magnetic dish assembly was attached to a small dc motor with a 1:2048 gear reducer and mounted at a small angle (less than 5°) from horizontal so that liquid in the dish gently flowed over the magnets as the dish rotated at ~0.25 rpm. The dish was loaded with only ~10 mL of SWCNT suspension to allow close contact of liquid with the magnet surfaces, sealed with plastic film to retard evaporation, and rotated for 30 min.

For further purification, the supernatant from first-stage processing was carefully withdrawn using a pipet and transferred to a second magnetic rotor device constructed from a 70 mm diameter, 50 mm deep crystallizing dish containing a circular array of 18 smaller disk magnets (9.4 mm diameter, 5 mm thick, N42 strength). These were also secured by magnetic attraction through the dish bottom to thin steel retaining plates. As shown in Figure 1, a 31 mm outer diameter acrylic tube was coaxially mounted and sealed inside the dish with silicone adhesive. This reduced the volume available to the sample and kept it in regions close to the magnets for faster purification. Similar to the first-step rotor, this device was also mounted to a gear-reduced dc motor for slow tilted rotation during second-step purification, which typically lasted for 4−5 h. Each magnetic rotor consumes only ~15 mW of power during operation. Approximately 85% of the initial sample volume was recovered after processing.

2.4. Sample Characterization. *2.4.1. Optical Spectroscopy.* We measured optical absorption and near-IR fluorescence spectra using a model NS2 NanoSpectralyzer (Applied NanoFluorescence, Houston, TX). Absorption spectra of aqueous SWCNT samples in 1.0 cm path length cells were recorded relative to a matched reference from 400 to 1400 nm, with spectral resolutions of 1 nm in the visible and 4 nm in the near-IR. These spectra are displayed without background subtraction or vertical offset. Fluorescence emission spectra were measured using diode laser excitation sources at 642, 659, and 784 nm. Raman spectra of the aqueous suspensions were obtained using a model NS3 NanoSpectralyzer (Applied NanoFluorescence, Houston, TX) with 671 nm excitation, or a model inVia Raman microscope (Renishaw) with 785 nm excitation.

2.4.2. Near-IR Fluorescence Microscopy. Dilute SWCNT suspensions were drop-cast onto glass slides and mounted on the sample stage of a Nikon TE-2000U inverted microscope that had been customized for near-IR fluorescence imaging, as described previously.[20] We used a 785 nm excitation laser and a 60× water-immersion objective lens (Nikon PlanApo IR, NA = 1.27). To help distinguish emissions of individual and aggregated SWCNTs, image sequences were recorded with a 100 ms exposure time while the excitation beam polarization plane was rotated in 10° steps. We then analyzed the depth of intensity modulation caused by polarization rotation for each emissive object in the frame. Spectra of single emissive objects in the SWCNT samples were also captured by a near-IR spectrometer coupled to the microscope. These spectra were examined for the presence of single or multiple emission peaks to help distinguish individual SWCNTs from aggregates.

dx.doi.org/10.1021/jp411941k | J. Phys. Chem. C 2014, 118, 4489−4494

2.4.3. Atomic Force Microscopy (AFM). To obtain AFM images of nanotubes in our samples, the DOC surfactant concentration of a suspension was decreased to 0.3% (w/v) by diluting with water. Then a small (ca. 10 μL) portion was spin-coated onto a freshly cleaved mica surface, passively dried for 1 min, washed with 10 μL of methanol to remove excess surfactant from the mica surface, and spun for another 5 min. The AFM image was acquired over a $(10\ \mu m)^2$ area with 512 samples/line resolution in tapping mode using a NanoScope IIIA (Digital Instruments). With the height profile range set to 5 nm, these AFM images were used to estimate the percentage of SWCNTs deposited as individual tubes from the purified suspension, and to measure SWCNT lengths.

2.4.4. Thermogravimetric Analysis (TGA). Thermogravimetric analysis of as-produced HiPco SWCNTs was performed by heating 2 mg samples to 800 °C in the presence of air in a model Q-600 Simultaneous TGA/DSC instrument (TA Instruments). To analyze magnetically purified SWCNTs, the surfactant was removed from processed samples suspended in aqueous DOC by repeated centrifugal filtration and washing (10K MWCO Nanosep filters, Pall Corp.). The filtered uncoated nanotubes were then oven-dried and collected as a pellet for analysis. We deduced Fe contents in the SWCNT samples by assuming that the residual mass in TGA runs represented Fe_2O_3.

3. RESULTS AND DISCUSSION

We studied the effect of magnetic processing by comparing properties of the HiPco HPR 188.4 suspensions before and after treatment, and also by examining small samples withdrawn periodically during the processing. Characterization methods included bulk optical absorption, near-IR fluorescence, and Raman spectroscopies; TGA measurements; microscopy using AFM and near-IR fluorescence imaging; and near-IR fluorescence spectroscopy of single particles. Figure 2 shows

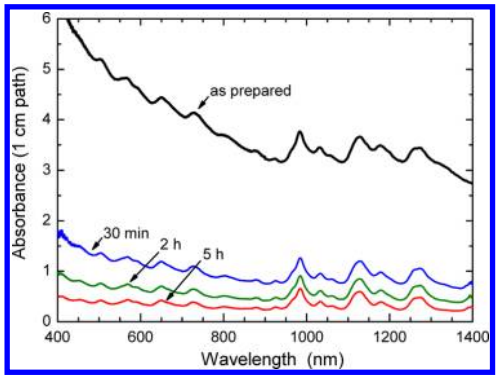

Figure 2. Changes in visible-near IR absorption due to magnetic purification processing. The top (black) trace shows the spectrum of the dispersed sample before processing, and the three lower traces show the sample's spectra after the labeled durations of processing.

the dramatic change in the absorption spectrum between the initial sample and the supernatant obtained from magnetic processing (see Figure S1 in the Supporting Information for the same data normalized to the 984 nm peak). The broad underlying background absorption dropped by a factor of approximately 10 after 5 h of processing, while resonant features identifiable as the E_{11} and E_{22} transitions of specific (n,m) species were only moderately reduced, suggesting retention of most individualized nanotubes. This increase in spectral contrast is also clear from Figure 3, which plots the difference between absorbance at the 984 nm peak and the

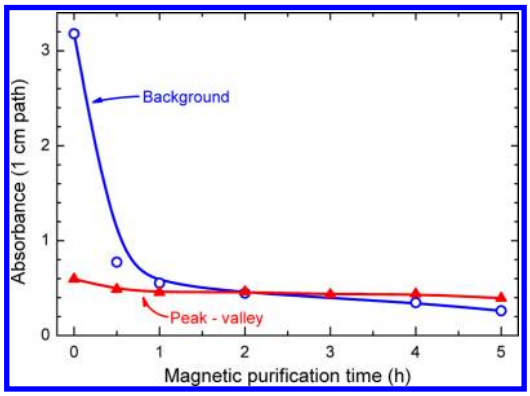

Figure 3. Absorbance spectral changes for the dispersed SWCNT sample during magnetic purification processing, as monitored at the 984 nm peak and 941 nm valley. Open circles (blue) show the 941 nm valley absorbance, signifying background absorption; closed triangles (red) show the peak-minus-valley absorbance difference, assigned to resonant SWCNT absorption. Processing decreases the background much more than the resonant signal.

adjacent 941 nm valley (to represent resonant absorption), and also the 941 nm absorbance (to represent the background component). The results imply that processing retains ~66% of the material giving sharp absorption features while removing 92% of material responsible for the broad background. We suspect that much of the removed background arose from tight SWCNT bundles with strong intertube electronic coupling, greatly broadened absorption features, and weak or absent emission. Changes in the measured fluorescence intensity reflect not only retention of emissive nanotubes but also removal of nonemissive components, including bundles and impurities, that can hinder light penetration through the sample. To correct for this inner filter effect, we have measured fluorescence spectra after adjusting the sample concentrations to give matched absorbance at the excitation wavelength. These results, which are plotted in Figures 4 and S14, reveal a nearly

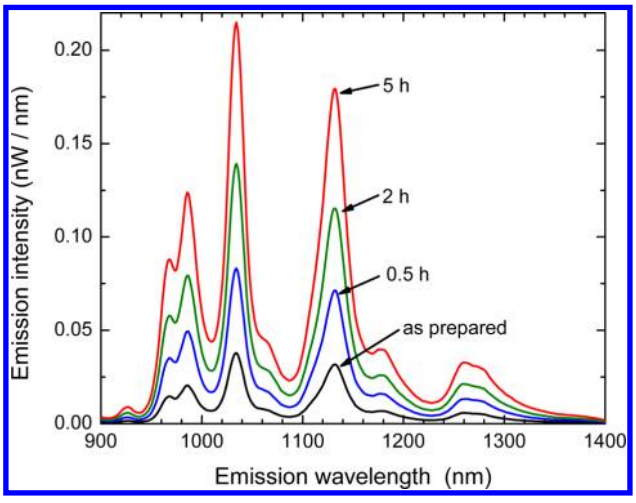

Figure 4. Fluorescence emission spectra (excited at 642 nm) for an as-prepared SWCNT sample and the same sample after various durations of magnetic processing and dilution to give matched absorbance at 642 nm for all measurements.

dx.doi.org/10.1021/jp411941k | J. Phys. Chem. C 2014, 118, 4489−4494

sixfold increase in average emission efficiency over 5 h of processing. This increase indicates selective removal of nonemissive components. Raman spectra with 671 nm excitation measured before and after magnetic processing show no significant differences in shape (Figure S2). However, 785 nm Raman spectra reveal that an RBM peak near 267 cm^{-1} is present in as-prepared samples but nearly absent after processing (Figure S3). This "roping" feature has been attributed to a bundling-induced shift of (10,2) SWCNTs into E_{22} resonance with the 785 nm excitation.[21] Its strong suppression by both magnetic processing and ultracentrifugation suggests comparable removal of nanotube bundles by the two purification methods.

To demonstrate that magnetic processing is useful for a variety of nanotube samples, we have obtained spectroscopic evidence of similar purification for a DOC suspension of HiPco SWCNTs from a batch containing less residual iron (Figure S4), and of HiPco HPR 188.4 nanotubes suspended in aqueous SDBS instead of DOC (Figure S5). Magnetic purification induced somewhat smaller spectral changes in SWCNT samples grown by the CoMoCAT method, which uses the ferromagnetic metal cobalt in its catalyst (Figure S6), and in larger diameter SWCNT samples grown by the plasma torch method (Figure S7). The higher final background absorptions in these two samples may reflect higher intrinsic defect densities.

We applied thermogravimetric analysis (TGA) to find the amount of Fe catalyst present in the HiPco HPR 188.4 samples before and after magnetic purification (Figure S8). On the basis of the residual mass values remaining after high-temperature oxidation and the assumption that iron is converted into Fe_2O_3, we found that the mass fraction of iron was reduced from 36% to ~12% by magnetic processing. It seems likely that refinements to the processing device and protocol could provide improved iron removal from the SWCNT dispersions.

The changes in optical absorption, emission, and Raman spectra suggest that our process for removing magnetic particles also removes nanotube aggregates from the supernatant. To investigate this point, we used near-IR fluorescence microscopy to study diluted supernatant samples drop-cast onto slides. Such samples may contain four relevant types of nano-objects: (1) individual fluorescent SWCNTs, with familiar sharp absorption and emission spectra; (2) fluorescent (small) bundles of parallel and strongly coupled SWCNTs, with broad absorption and perturbed or quenched emission spectra; (3) aggregates containing emissive SWCNTs that are weakly electronically coupled and not aligned with each other, showing sharp spectral features at multiple wavelengths; and (4) nonfluorescent SWCNTs in the form of individuals, bundles, or aggregates. A specific signature that distinguishes individual or small bundled SWCNTs from weak aggregates is strong modulation of emission intensity when the excitation polarization plane is rotated. Approximately 80% of the objects observed in fluorescence microscopy of a magnetically processed sample showed such modulation (Figure 5a,b), whereas comparison samples showed modulation in only 24% of objects before purification but 86% after ultracentrifugation (Figure S18a). We also measured emission spectra of 100 randomly chosen emitters in the magnetically processed sample. Of these, 82 showed single-peaked spectra indicating individual or small bundled SWCNTs (Figures S9 and S17b) whereas 18 gave more complex spectra consistent with weakly coupled aggregates (Figures S10 and S17c). For comparison,

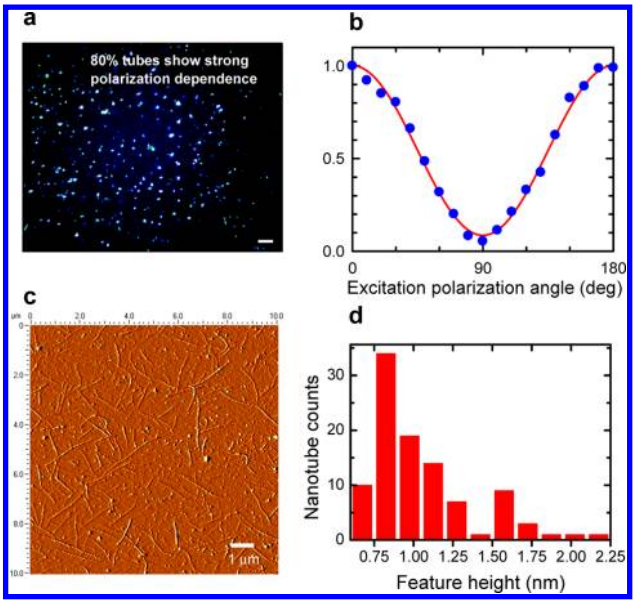

Figure 5. Microscopic characterization of magnetically purified SWCNT samples. (a) Near-IR fluorescence micrograph of magnetically purified SWCNTs drop-cast on a glass microscope slide. Scale bar length is 5 μm. (b) Spectrally integrated intensities from an individual emissive object in the microscope field as a function of excitation beam polarization angle. The solid curve shows a $\cos^2$ fit to the data points. (c) AFM image (amplitude profile) of magnetically purified SWCNTs spin-coated on a mica surface. (d) Height histogram of nanotubes in the AFM image. Approximately 76%–80% of objects appear to be individual nanotubes rather than aggregates.

the fraction of emissive objects showing single-peaked spectra was only 30% in an unpurified SWCNT dispersion (Figure S17) but 84% in an ultracentrifuged sample. These results indicate that magnetic processing and ultracentrifugation are similarly effective in removing emissive nanotube aggregates.

We supplemented these optical measurements with AFM images of the magnetically processed supernatant (Figures 5c and S11). As shown in Figure 5d, the distribution of measured AFM height profiles appears bimodal, with a main peak near 0.8 nm and a secondary peak near 1.6 nm. Presuming that objects with apparent heights of 1.1 nm or less represent single SWCNTs, approximately 76% of the AFM-imaged features can be assigned to individualized nanotubes. A similar analysis of unprocessed and ultracentrifuged dispersions found 21% and 85% apparent individualized nanotubes, respectively (Figures S15 and S16). Both optical and AFM microscopy therefore indicate that magnetic purification is nearly as effective as ultracentrifugation in removing nanotube aggregates and enriching supernatants in individualized nanotubes. The average nanotube length found from AFM image analysis is approximately 1.1 μm (Figure S12). This relatively large value reflects the moderate sonication conditions used for dispersing this sample prior to magnetic treatment, but our purification method is also effective with more strongly sonicated samples.

Since 2002,[6] ultracentrifugation has served as the standard method for removing aggregates from SWCNT dispersions to enrich samples in individualized nanotubes. To further compare the effectiveness of ultracentrifugation and magnetic purification, we present in Figure 6 the optical absorption spectra of SWCNT supernatants prepared from the same starting HiPco dispersion using both methods. The two spectra are very similar in magnitude and shape, although the nonresonant background

dx.doi.org/10.1021/jp411941k | J. Phys. Chem. C 2014, 118, 4489–4494

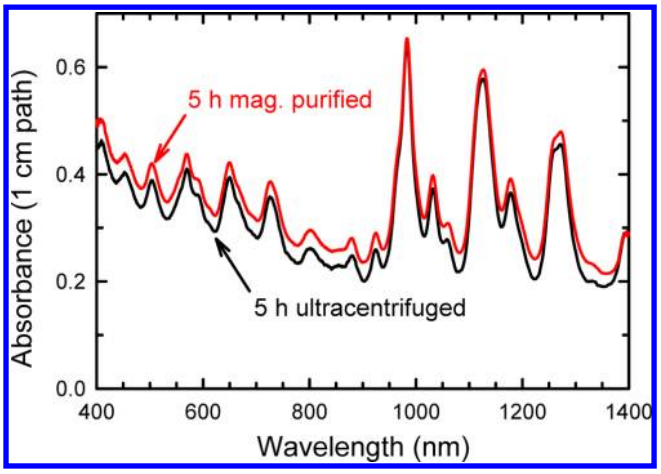

Figure 6. Comparison of visible-near IR absorption spectra for magnetically processed and ultracentrifuged SWCNT samples. Upper (red) trace shows supernatant spectrum of a nanotube dispersion purified by 5 h of magnetic processing; lower (black) trace shows supernatant spectrum of the same dispersion ultracentrifuged for 5 h at 171 000*g*.

is ~12% higher in the magnetically processed sample, indicating slightly less efficient aggregate removal. Figure 7 compares

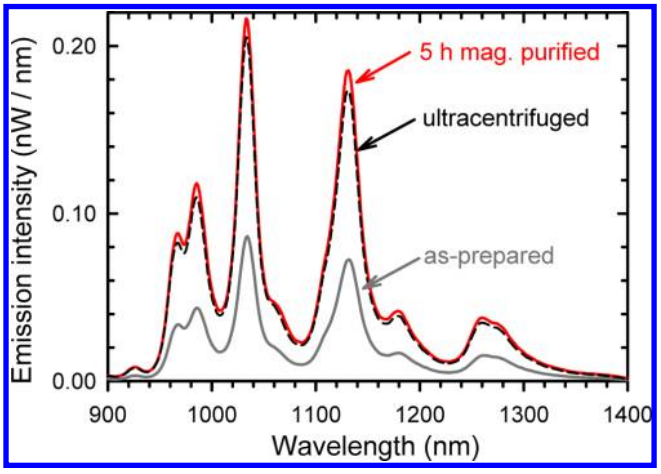

Figure 7. Supernatant fluorescence emission spectra (with 642 nm excitation) from the magnetically processed (red trace) and ultracentrifuged (black trace) samples under matched conditions. The emission spectrum of the unprocessed SWCNT dispersion is also shown for comparison.

fluorescence emission spectra of the processed samples measured under matched conditions. The two traces are almost identical. They both show emission that is much more intense than from the parent unprocessed dispersion, reflecting the removal of absorbing but nonemissive impurities. These spectral measurements, which are known to sensitively reflect SWCNT condition, aggregation state, and impurity content, support our conclusion that magnetic purification of raw HiPco product can give samples comparable in quality to those prepared by lengthy ultracentrifugation.

Finally, we have examined the solid residue deposited on the permanent magnets during processing. Deposits are found to be densest along edges of the magnets, where the magnetic field gradients are largest and forces on ferromagnetic particles are expected to be greatest. When this solid residue was gently redispersed with manual agitation, it gave suspensions whose absorption spectra show large diffuse backgrounds and weaker resonant features than the unprocessed sample (Figure S19). The redispersed residue also gave fluorescence intensities that were much lower (by a factor of ~13) as compared to a processed sample with equal absorbance at 980 nm (Figure S20). Although we cannot rule out the possibility that surfactant-coated nanotubes in the residue became aggregated during deposition onto the magnet faces, it seems more likely that the magnetic forces simply captured pre-existing aggregates from the suspension. In this case, the spectra in Figures S19 and S20 further support the hypothesis of a purification process that disproportionately removes nanotube aggregates and impurities. In a speculative mechanistic model for this selectivity, we note that the raw sample may contain carbon-coated catalytic iron nanoparticles in several forms: as separate objects; or noncovalently linked to bundles and aggregates through multipoint interactions; or covalently attached during growth to SWCNTs that may be individualized or bundled. A larger fraction of bundles and aggregates than individuals would contain at least one iron particle. Magnetic processing could then preferentially trap such species along with unattached iron particles, leaving supernatants relatively enriched in individually suspended nanotubes. Further experimental studies will be needed to test this suggestion and clarify the mechanism of magnetic aggregate removal.

4. CONCLUSIONS

Using a range of bulk and single-particle characterization methods, we have demonstrated a simple nanotube purification method in which aqueous dispersions of raw SWCNTs are gently circulated over permanent magnets. The resulting supernatants retain most of the individualized SWCNTs but are strongly depleted not only in residual ferromagnetic catalyst but also in aggregated nanotubes. Optical properties of these samples are comparable to those of supernatants prepared by extensive ultracentrifugation. However, the new processing method should offer major advantages in equipment cost, simplicity, energy usage, and scalability. We expect that it will prove useful for laboratory research and industrial applications.

■ ASSOCIATED CONTENT

Supporting Information

Plots of additional absorption, fluorescence, and Raman spectral data; TGA data; single-particle emission spectra; AFM images; SWCNT length histogram; spectra of material removed by magnets; data showing purification of SWCNTs from different growth processes and in a different surfactant. This material is available free of charge via the Internet at http://pubs.acs.org.

■ AUTHOR INFORMATION

Corresponding Author

*E-mail: weisman@rice.edu.

Notes

The authors declare the following competing financial interest(s): R.B.W. has a financial interest in Applied NanoFluorescence, LLC, the manufacturer of one instrument used in this study.

■ ACKNOWLEDGMENTS

This research was supported by grants from the National Science Foundation (CHE-1112374) and the Welch Foundation (C-0807). We thank R. H. Hauge for useful discussions and X. Fan for assistance with TGA measurements.

■ REFERENCES

(1) Itkis, M. E.; Perea, D. E.; Jung, R.; Niyogi, S.; Haddon, R. C. Comparison of Analytical Techniques for Purity Evaluation of Single-Walled Carbon Nanotubes. *J. Am. Chem. Soc.* **2005**, *127*, 3439−3448.
(2) Graupner, R. Raman Spectroscopy of Covalently Functionalized Single-Wall Carbon Nanotubes. *J. Raman Spectrosc.* **2007**, *38*, 673−683.
(3) Naumov, A. V.; Ghosh, S.; Tsyboulski, D. A.; Bachilo, S. M.; Weisman, R. B. Analyzing Absorption Backgrounds in Single-Walled Carbon Nanotube Spectra. *ACS Nano* **2011**, *5*, 1639−1648.
(4) Cognet, L.; Tsyboulski, D.; Rocha, J.-D. R.; Doyle, C. D.; Tour, J. M.; Weisman, R. B. Stepwise Quenching of Exciton Fluorescence in Carbon Nanotubes by Single-Molecule Reactions. *Science* **2007**, *316*, 1465−1468.
(5) Strano, M. S.; Moore, V. C.; Miller, M. K.; Allen, M. J.; Haroz, E. H.; Kittrell, C.; Hauge, R. H.; Smalley, R. E. The Role of Surfactant Adsorption During Ultrasonication in the Dispersion of Single-Walled Carbon Nanotubes. *J. Nanosci. Nanotechnol.* **2003**, *3*, 81−86.
(6) O'Connell, M. J.; Bachilo, S. M.; Huffman, C. B.; Moore, V.; Strano, M. S.; Haroz, E.; Rialon, K.; Boul, P. J.; Noon, W. H.; Kittrell, C.; et al. Band-Gap Fluorescence From Individual Single-Walled Carbon Nanotubes. *Science* **2002**, *297*, 593−596.
(7) Thien-Nga, L.; Hernadi, K.; Ljubovic, E.; Garaj, S.; Forro, L. Mechanical Purification of Single-Walled Carbon Nanotube Bundles From Catalytic Particles. *Nano Lett.* **2002**, *2*, 1349−1352.
(8) Wiltshire, J. G.; Li, L. J.; Khlobystov, A. N.; Padbury, C. J.; Briggs, G. A. D.; Nicholas, R. J. Magnetic Separation of Fe Catalyst Form Single-Walled Carbon Nanotbues in an Aqueous Surfactant Solution. *Carbon* **2005**, *4*, 1151−1155.
(9) Kang, J. H.; Park, J. K. Magnetophoretic Continuous Purification of Single-Walled Carbon Nanotubes From Catalytic Impurities in a Microfluidic Device. *Small* **2007**, *3*, 1784−1791.
(10) Kang, J. H.; Park, J. K. In *An microfluidic magnetophoresis chip for continuous single-walled carbon nanotube purification from magnetic force-induced superparamagnetic metal catalyst*, Proceedings of MEMS 2007 Conference, Jan 21, 2007; IEEE: Piscataway, NJ, 2007; pp 437−440.
(11) Zheng, M.; Jagota, A.; Strano, M. S.; Santos, A. P.; Barone, P. W.; Chou, S. G.; Diner, B. A.; Dresselhaus, M. S.; McIean, R. S.; Onoa, G. B.; et al. Structure-Based Carbon Nanotube Sorting by Sequence-Dependent DNA Assembly. *Science* **2003**, *302*, 1545−1548.
(12) Zheng, M.; Semke, E. D. Enrichment of Single Chirality Carbon Nanotubes. *J. Am. Chem. Soc.* **2007**, *129*, 6084−6085.
(13) Arnold, M. S.; Stupp, S. I.; Hersam, M. C. Enrichment of Single-Walled Carbon Nanotubes by Diameter in Density Gradients. *Nano Lett.* **2005**, *5*, 713−718.
(14) Arnold, M. S.; Green, A. A.; Hulvat, J. F.; Stupp, S. I.; Hersam, M. C. Sorting Carbon Nanotubes by Electronic Structure Using Density Differentiation. *Nat. Nanotechnol.* **2006**, *1*, 60−65.
(15) Ghosh, S.; Bachilo, S. M.; Weisman, R. B. Advanced Sorting of Single-Walled Carbon Nanotubes by Nonlinear Density-Gradient Ultracentrifugation. *Nat. Nanotechnol.* **2010**, *5*, 443−450.
(16) Tanaka, T.; Urabe, Y.; Nishide, D.; Kataura, H. Continuous Separation of Metallic and Semiconducting Carbon Nanotubes Using Agarose Gel. *Appl. Phys. Express* **2009**, *2*, 125002.
(17) Liu, H.; Feng, Y.; Tanaka, T.; Urabe, Y.; Kataura, H. Diameter-Selective Metal/Semiconductor Separation of Single-Wall Carbon Nanotubes by Agarose Gel. *J. Phys. Chem. C* **2010**, *114*, 9270−9276.
(18) Liu, H.; Nishide, D.; Tanaka, T.; Kataura, H. Large-Scale Single-Chirality Separation of Single-Wall Carbon Nanotubes by Simple Gel Chromatography. *Nat. Commun.* **2011**, *2*, 309.
(19) Bronikowski, M. J.; Willis, P. A.; Colbert, D. T.; Smith, K. A.; Smalley, R. E. Gas-Phase Production of Carbon Single-Walled Nanotubes From Carbon Monoxide Via the HiPco Process: A Parametric Study. *J. Vac. Sci. Technol.* **2001**, *A19*, 1800−1805.
(20) Tsyboulski, D. A.; Bachilo, S. M.; Weisman, R. B. Versatile Visualization of Individual Single-Walled Carbon Nanotubes With Near-Infrared Fluorescence Microscopy. *Nano Lett.* **2005**, *5*, 975−979.
(21) Heller, D. A.; Barone, P. W.; Swanson, J. P.; Mayrhofer, R. M.; Strano, M. S. Using Raman Spectroscopy to Elucidate the Aggregation State of Single-Walled Carbon Nanotubes. *J. Phys. Chem. B* **2004**, *108*, 6905−6909.